Molecular dynamics study of nematic structures confined to a cylindrical cavity

Z. Bradač,[1] S. Kralj,[1,2] and S. Žumer[2]
[1]*Department of Physics, Faculty of Education, University of Maribor, Koroška 160, 2000 Maribor, Slovenia*
[2]*Department of Physics, FMF, University of Ljubljana, Jadranska 19, 1000 Ljubljana, Slovenia*
(Received 10 August 1998)

Molecular dynamics is used to simulate nematic liquid crystal structures confined to a submicron cylindrical cavity. Molecules, fixed at the lattice points, are set to interact via a modified induced-dipole–induced-dipole type coupling. Stability regions of characteristic nematic structures are determined as functions of the cylinder radius, homeotropic anchoring strength, and degree of the interaction anisotropy. A connection linking elastic and microscopic approaches is established. Results confirm most of the predictions of the elastic free energy deep in the submicron regime. [S1063-651X(98)06112-1]

PACS number(s): 61.30.Cz, 61.30.Gd, 64.70.Md

I. INTRODUCTION

In recent years nematic liquid crystals (LC's) confined into cylindrical cavities attracted a lot of attention. Confined nematic structures were examined mostly by optic polarization microscopy [1–3] in supramicron and NMR methods [4,5] in submicron cavities. The findings are in reasonable agreement with the predictions based on phenomenological theories [6,7].

In cavities of radius $R>1$ μm most of theoretical studies were carried out within the uniaxial approximation [6,8,9] in terms of the director field $\vec{n}$ and the nematic order parameter S. As the nematic order parameter correlation length ξ_n was usually much less than R the order parameter S has a nearly constant value everywhere except close to the centers of defects [10]. In such cavities the approximation of constant order parameter works well, while defects are described by an isotropic core whose linear dimension is roughly given by ξ_n.

This approach is not appropriate for cavities with a diameter well below 1 μm, which have recently been of particular research interest. There have been numerous studies devoted to liquid crystals confined to porous matrices [11] (e.g., Anopore [12] and Nuclepore [13] membranes, aerogels [14], Russian glass [15], Vycor glass [16], controlled porous glass [17], etc.), with typical voids in most cases locally exhibiting a roughly cylindrical geometry of a radius well below 1 μm. In such cavities spatial variations of the nematic order parameter are prominent, and in addition biaxiality becomes apparent. In most cases a more complex continuum approach based on the tensor nematic order parameter [7] is needed.

However, approaching molecular scales the applicability of continuum type descriptions becomes questionable [18]. Zannoni and co-workers pioneered molecular simulation approaches for confined liquid crystals [18–23]. Palermo, Biscarini, and Zannoni demonstrated [21] a breakdown of standard continuum theory using Gay-Berne potential studying orientational changes of LC's adsorbed on a graphite surface. They observed large director variations in the proximity of the surface, which cannot be tackled with continuum type approaches. On the other hand some of their result confirm some of elastic predictions (i.e., details concerning paranematic-nematic phase transition and existence of various nematic structures within spherically and cylindrically shaped cavities) [19,20,22–25]. A connection between elastic and molecular descriptions was partially established. In particular the question of the length scale entering the model (i.e., how many molecules in the real world correspond to a lattice point in the microscopic description) was not answered.

The main goals of this paper are (i) to use a simple microscopic description to investigate the stability of different nematic structures in a cylindrical cavity with walls enforcing homeotropic anchoring, and (ii) to establish a link with results of continuum type approaches. The LC molecules, fixed in a lattice, are assumed to be coupled via a modified induced-dipole–induced-dipole type interaction [26]. The relaxation of nematic structures toward (meta)stable configurations is enabled using a molecular dynamics simulation [27]. The paper is organized in the following way. In Sec. II the theoretical background is presented. We discuss possible nematic structures based on continuum predictions. The interaction between molecules is presented, and the method of molecular dynamics is briefly described. In Sec. III the stability of different nematic structures is studied as a function of anchoring strength, interaction anisotropy, and cylinder radius, emphasizing the link to the continuum description. In that section, results are also summarized.

II. THEORETICAL BACKGROUND

A. Nematic structures

A nematic structure in a cylindrical cavity results from a competition among surface, elastic and eventual external (magnetic or electric) field effects. Conditions at the confining boundary are of particular importance. In this study we limit ourselves to homeotropic [28] anchoring, tending to orient nematic molecules in the radial direction. Using topological arguments, possible structures can be qualitatively predicted [10,29–31]. In Figs. 1(a)–1(g), some structures are schematically represented using the nematic director field representation.

Planar director fields. In the case of strong homeotropic anchoring at the cylinder wall, and a planar director field

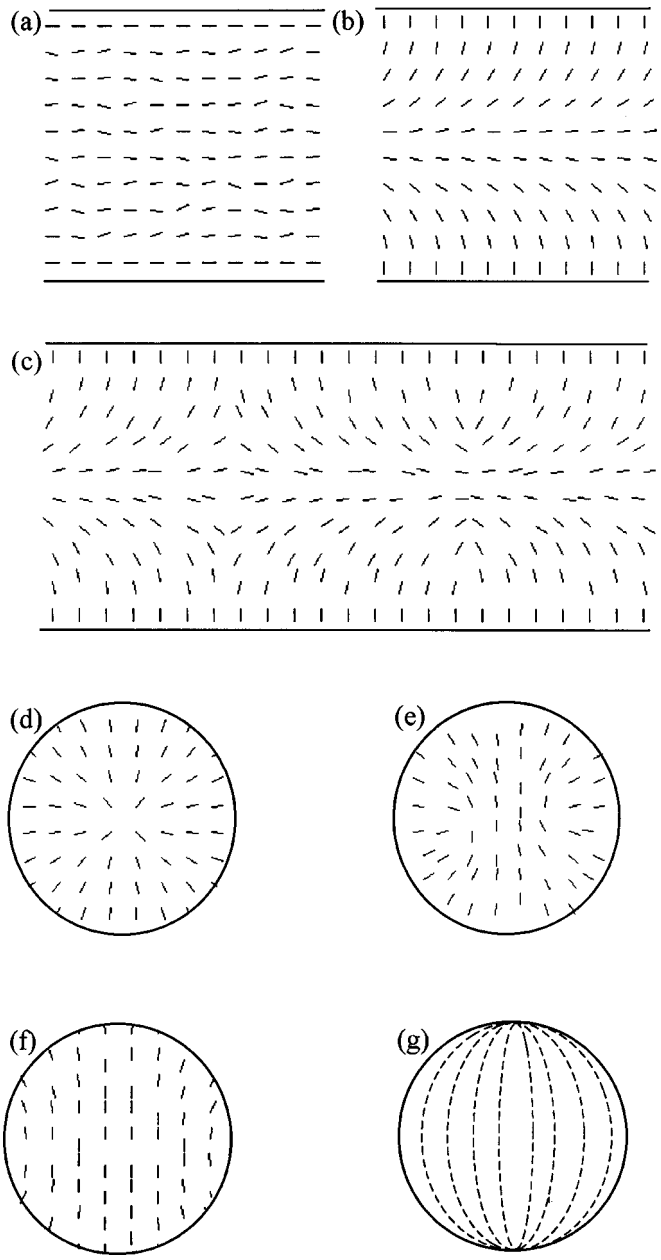

FIG. 1. Schematic sketch of the (a) axial homogeneous (AH), (b) escaped radial (ER), (c) escaped radial with point defects (ERPD), (d) planar radial (PR), (e) planar polar structure with line defects (PPLD), (f) planar polar (PP), and (g) planar bipolar (PB) nematic structure in the director field representation.

restricted to planes normal to the cylinder axis, the defects are topologically required. Defects are conventionally classified according to their topological charge M (on encircling a defect the director field rotates for an angle $M2\pi$). For strong homeotropic anchoring the sum of topological charges in any possible structure is restricted to 1 [31]. The simplest scenario, that can potentially result in a stable structure, corresponds to the planar radial [6] (PR) structure possessing a single line defect of strength $M=+1$. Also, structures with a two line defect of the strength $M=+\frac{1}{2}$ are possible. Because of the same sign the defects repel each other, and at the same time they are also repelled from the curved surface (its presence can be simulated by a mirror image defect). The structure, where defects are stabilized at a finite mutual distance, is conventionally called the planar polar structure [8] with two line defects (PPLD). Structures with even more defects, subject to given constraints, are too energetic to be stable. In case of a finite anchoring strength these defects can be virtually pushed out of the cylinder resulting in the defectless planar polar (PP) structure [6].

Escaped director fields. The additional degree of freedom along the cylinder axis enables the system to avoid line defects also in the strong anchoring regime via ''the escape in the third dimension'' [1,10]. Possible scenaria are the escaped radial [6] (ER) structure and the escaped radial structure with point defects [6,32] (ERPD). On decreasing the anchoring strength the ER structure exhibits a continuous transition to the axial homogeneous [6] (AH) structure. Other structures, e.g., including twist nematic distortion [33], are only rarely realized.

B. Stability of structures: elastic theory prediction

In the continuum limit the stability region of the structures mentioned above can be well predicted knowing ratios of typical lengths entering the problem [6–8]. These are the cylinder radius R, the surface extrapolation length [7] d_e, the nematic correlation length ξ_n, and the external field correlation length [7] ξ_f. In addition, relative strengths of the splay (K_{11}), twist (K_{22}), bend (K_{33}), and saddle splay (K_{24}) nematic elastic constant can play important roles [6–8].

Supramicron range. We first consider supramicron cavities corresponding to the regime $R/\xi_n \gg 1$. In this limit the uniaxial elastic Frank-Oseen type description [7] in terms of a constant nematic order parameter works well.

For comparable nematic elastic constants and in the absence of an external field, only the ER and PP structures can be stable [6,8]. The PP structure is stable if $R/d_e < (R/d_e)_c = \mu_c$ (weak anchoring regime), and the ER structure if $R/d_e > \mu_c$ (strong anchoring regime). Here μ_c describes the critical value [6,8] which depends on the relative strength of nematic elastic constants. For equal elastic constants $\mu_c \simeq 10$. Despite the fact that the ER structure is slightly less energetic than topologically equivalent metastable ERPD structure, the ERPD structure is most commonly experimentally observed instead. Possible origins of its stability were discussed in detail by Peroli and Virga [32]. The PR structure is stable only if, in addition to $R/d_e > \mu_c$, the condition $K_{33}/K_{11} \gg 1$ is also realized [8]. This can occur in conventional nematics close to the continuous nematic-smectic A phase transition. An external field applied perpendicular to the cylinder axis can stabilize the PP structure also in the strong anchoring regime if the ratio $d_e/\xi_f > (d_e/\xi_f)_c$, where the subscript c stands for the critical value. In the very strong anchoring regime ($R/d_e \gg 10$) there exists a limited interval [8] of external field strengths where the PPLD structure is stable. Note that in the $(R/d_e, d_e/\xi_f)$ stability diagram the lines separating defectless structures exhibit scaling properties [6,8].

Submicrometer range. In the submicron range, where R and the nematic order parameter correlation length ξ_n are comparable, a more detailed description of defects has to be introduced. This was taken into account in Ref. [24] using

the tensor nematic order parameter description. In this picture biaxiality is allowed. According to these results in the strong anchoring regime the PPLD (or even PR) structure is realized instead of the ER one even for equal nematic elastic constants if $R<20\xi_0$. Here ξ_0 is the zero temperature nematic correlation length [7] (for MBBA, LC $\xi_0 \approx 1$nm). Similar conclusions were reached by [25] Ziherl and Zumer studying the stability of the PR structure from dynamic point of view in the uniaxial approximation, allowing a spatial variation of the nematic orientational order parameter. The Monte Carlo study [20] by Chiccoli *et al.*, based on a Lebwohl-Lasher [34] microscopic model, suggested that some of the predictions obtained via continuum approaches work well also in the submicron regime. They observed a PPLD-like structure for strong enough anchoring. The size of their sample was too small to obtain other structures predicted by continuum theories.

C. Microscopic interaction

Within the model a pair of rodlike LC molecules (more exactly, an average representative [18,23] of a cloud of molecules) fixed at $\vec{r}_1$ and $\vec{r}_2$, whose orientation is described by $\vec{n}_1$ and $\vec{n}_2$, interact via a simple pairwise interaction [26,35]

$$f(\vec{n}_1,\vec{n}_2,\vec{r}) = -\frac{J}{r^6}\left(\vec{n}_1\cdot\vec{n}_2 - \frac{3\varepsilon}{r^2}(\vec{n}_1\cdot\vec{r})(\vec{n}_2\cdot\vec{r})\right)^2. \quad (1)$$

This interaction corresponds to the generalized van der Waals interaction. Here $\vec{r}=\vec{r}_2-\vec{r}_1$, and J is a positive interaction constant. The parameter ε describes the degree of orientational anisotropy. For $\varepsilon=0$ the isotropic (i.e., independent of the $\vec{r}$ direction) Maier-Saupe interaction is obtained. This interaction is usually presented in a slightly different form, where the term $(\vec{n}_1\cdot\vec{n}_2)^2$ in replaced by $P_2(\vec{n}_1\cdot\vec{n}_2)$, where P_2 is a second rank Legendre polynomial. The corresponding coupling is called the Lebwohl-Lasher [34] pair potential.

The induced dipole-induced dipole type interaction emerges for $\varepsilon = 1$. The basic properties of this model are given in Ref. [34]. It reasonably describes properties of nematic liquid crystals for $\varepsilon \leqslant 0.3$.

The molecules are coupled with the enclosing surface via [20]

$$f_s(\vec{n},\vec{r}) = -\frac{J_s}{r^6}(\vec{n}\cdot\vec{e}_s)^2, \quad (2)$$

where $\vec{r}$ is the distance between a ''molecule'' and a chosen point at the surface. J_s is a positive surface anchoring constant tending to orient nematic molecules along the easy axis $\vec{e}_s$. In this study, $\vec{e}_s$ points in the radial direction, corresponding to the so called homeotropic [28] anchoring. The interaction energy $W_{\rm int}$ of the whole sample is given as a sum over all pair interactions. In calculations we limit ourselves only to first neighbors. In addition we limit ourselves to relatively low temperatures, where $W_{\rm int}$ and the free energy are almost equal.

D. Molecular dynamics study

We study the stability of nematic structures within a cylindrical cavity whose lateral wall enforces homeotropic anchoring (the easy axis points along the surface normal). The director field is parametrized as

$$\vec{n} = \vec{e}_x\sin\Theta\cos\Phi + \vec{e}_y\sin\Theta\sin\Phi + \vec{e}_z\cos\Theta, \quad (3)$$

where $\Theta=\Theta(\vec{r},t)$ and $\Phi=\Phi(\vec{r},t)$ are the variational parameters given at a discrete time t and points $\vec{r}=(x,y,z)$ of the Cartesian coordinate system. Thus discarded twist-nematic deformations are also conventionally allowed. The molecules are fixed in a cubic three-dimensional lattice of lattice spacing a_o. The nematic is confined within a cylinder of radius $R=N_r a_o$ and length $L=N_z a_o$. In the simulation all the 26 first neighbors of a ''molecule'' centered at a site $\vec{r}$ whose orientation is to be updated were taken into account (i.e., eight ''molecules'' in the central plane including the site $\vec{r}$, and nine ''molecules'' at the plane above and below the central plane). In the evaluation of the torque on the ''molecule'' at $\vec{r}$ all these neighbors were mapped on a sphere of radius a_o centered at $\vec{r}$. In such a way we get rid of the preference axis introduced into the system via the choice of a cubic lattice [35].

The director field orientation is updated in a time interval Δt via [36]

$$\Theta(x,y,z,t+\Delta t) = \Theta(x,y,z,t) - \Delta t A\frac{\partial W_{\rm int}}{\partial\Theta} + \Theta_r, \quad (4)$$

$$\Phi(x,y,z,t+\Delta t) = \Phi(x,y,z,t) - \Delta t A\frac{\partial W_{\rm int}}{\partial\Phi} + \Phi_r. \quad (5)$$

The constant A depends on temperature and viscous properties of the liquid crystal system [36]. The derivatives entering Eqs. (4) are calculated as

$$\frac{\partial W_{\rm int}}{\partial\Theta} = \frac{W_{\rm int}(\Theta+\Delta\Theta,\Phi) - W_{\rm int}(\Theta-\Delta\Theta,\Phi)}{2\Delta\Theta}, \quad (6)$$

$$\frac{\partial W_{\rm int}}{\partial\Phi} = \frac{W_{\rm int}(\Theta,\Phi+\Delta\Phi) - W_{\rm int}(\Theta,\Phi-\Delta\Phi)}{2\Delta\Phi}, \quad (7)$$

where $\Delta\Theta$ and $\Delta\Phi$ are sufficiently small angles. The temperature T is introduced in the model via random variables Θ_r and Φ_r. The corresponding probabilities are described by Gaussian distributions centered at $\Theta=0$ and $\Phi=0$, respectively. The width of the distribution is proportional to T. Details are given in Ref. [37].

Simulations were carried for the sample sizes $(2R,L) \propto (2N_r,N_z) = (8,28)$, $(16,28)$, $(24,28)$, $(32,28)$, and $(32,44)$. At the cylindrical wall homeotropic anchoring is induced via coupling given by Eq. (2). The anchoring strength is varied from $J_s/J=0$ to 3.0. In the z direction at $z=0$ and $z=L$, periodic boundary conditions are assumed. The anisotropy parameter range from $\varepsilon=0$ to 0.3 is explored. Calculations were performed deep in the nematic phase. The structures were quenched from the isotropic

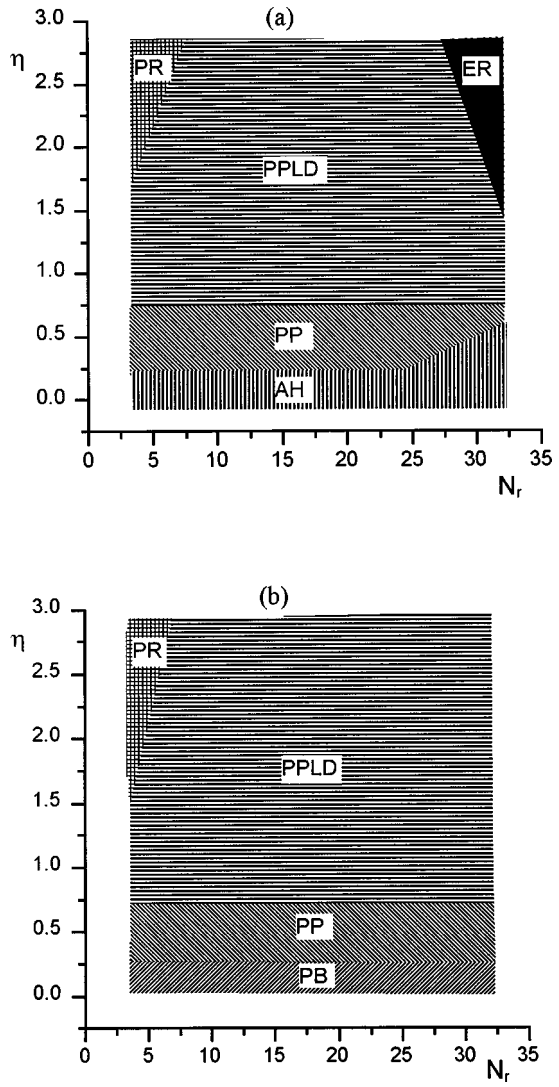

FIG. 2. The stability diagram $\eta = J_s/J$ as function of N_r for (a) $\varepsilon = 0$ and (b) $\varepsilon = 0.3$. Case (a) corresponds in the elastic description to the approximation of equal elastic constants.

phase and were typically stabilized after 10 000 sweeps (in one sweep the orientations of all the ''molecules'' are updated).

III. RESULTS AND DISCUSSION

A. Stability diagram

With the above mentioned range of parameters, six qualitatively different stable nematic structures are obtained. None of them exhibits twist-nematic distortions justifying the implemented assumptions in several recent theoretical continuum type simulations [6,8,24,38,39]. Note that twisted structures of nonchiral systems [33] can in principle be stable for a relatively low value of the Frank twist elastic constant K_{22} in comparison to K_{11} and K_{33}. However this realm can not be reached within our model where the relative strength of elastic constants is controlled [26] solely by ε. The corresponding stability diagrams $\eta = J_s/J$ as a function of N_r are shown in Fig. 2(a) ($\varepsilon = 0$) and 2(b) ($\varepsilon = 0.3$). The ratio η reflects competition between surface and elastic interaction strength.

$\varepsilon = 0$, *equal elastic constants.* We first discuss the isotropic case ($\varepsilon = 0$) that corresponds in the elastic description to the approximation of equal nematic elastic constants [40] ($K_{11} = K_{22} = K_{33} = K_{24} \equiv K$; $K_{13} = 0$). For small enough radia ($2N_r < 25$), there exist a critical value $\eta = \eta_c$ ($0 < \eta_c < 0.5$) separating regimes of qualitatively different nematic structures.

For $\eta < \eta_c$ the AH structure is stable (weak anchoring regime). At $\eta = \eta_c$ the anchoring is strong enough to stabilize the PP structure, which adopts to the homeotropic anchoring condition in a less energetic way. The points of maximal distortion are positioned diametrically at the wall. With increased ratio these points become more distorted but remain at the wall until a critical value $\eta = \eta_{c1}$ is reached. With a further increased value of η the localized distortions (i.e., line defects) are pushed toward the center of the cylinder, approaching a saturated value of $\Delta R_s = \Delta R(\eta \to \infty)$. Here $\Delta R(\eta)$ describes the shortest distance between the cylinder wall and the localized distortion (i.e., line defects in the director field description). This nematic configuration corresponds to the planar polar structure with line defects (PPLD) structure. If $\Delta R_s \approx R$ then PR structure is formed (see stability diagrams). This condition can be realized only for extremely small values of R and for high enough values of η.

The evolution of the nematic structure with increased η at constant value of R ($N_r = 8$) is illustrated in Fig. 3. The corresponding dependence $\Delta R(\eta)$ of the PPLD structure is plotted in Fig. 4. Note that one would expect a monotonically decreased value of the ratio $\Delta R_s/R$ with increased R. In this context minor departures from this tendency indicate the degree of reliability of calculations.

For large enough radia the planar structures are not stable, and the ER structure is realized instead for all anchoring strengths. This behavior is in line with elastic predictions [6,8] to which our result should converge in the limit $N_r \gg 10$. Details about this structure will be given below.

$\varepsilon = 0.3$, *intrinsic anchoring.* A finite value of the anisotropy constant ε introduces quantitative and qualitative changes into the stability diagram. When $\varepsilon > 0$, the degeneracy of equal elastic constants of the continuum approach is lifted [26,35], and in addition $K_{13} \neq 0$. It roughly holds [26] that $K_{13}/K \approx -3\varepsilon/5[-1+(9/7)\varepsilon]/[1-(12/5)\varepsilon + (54/35)\varepsilon^2]$. Consequently, in addition to *external anchoring,* the system also exhibits *internal anchoring,* which can result in deformed nematic structures. The internal anchoring [35] is caused by incomplete intermolecular interaction. Because of the curved surface it can cause deformed structure even in cases of $J_s = 0$.

Some of the resulting consequences are evidently manifested in Fig. 2(b). The stability of the ER structure is pushed toward higher values of N_r, indicating $K_{33}/K_{11} > 1$. The competing planar nematic structures exhibit less bend deformation in comparison to the ER director profile [8]. More remarkable is the appearance of a planar bipolar (PB)-like structure [9] in the very weak anchoring regime despite the homeotropic anchoring condition. Note that considering conventional bulk elastic constants, this structure can be stabilized only for a planar anchoring condition for considerable anchoring strength. The appearance of the PB structure in such a weak anchoring regime is due to intrinsic [35] anchoring. It is caused by finite value of *divergence* (also called

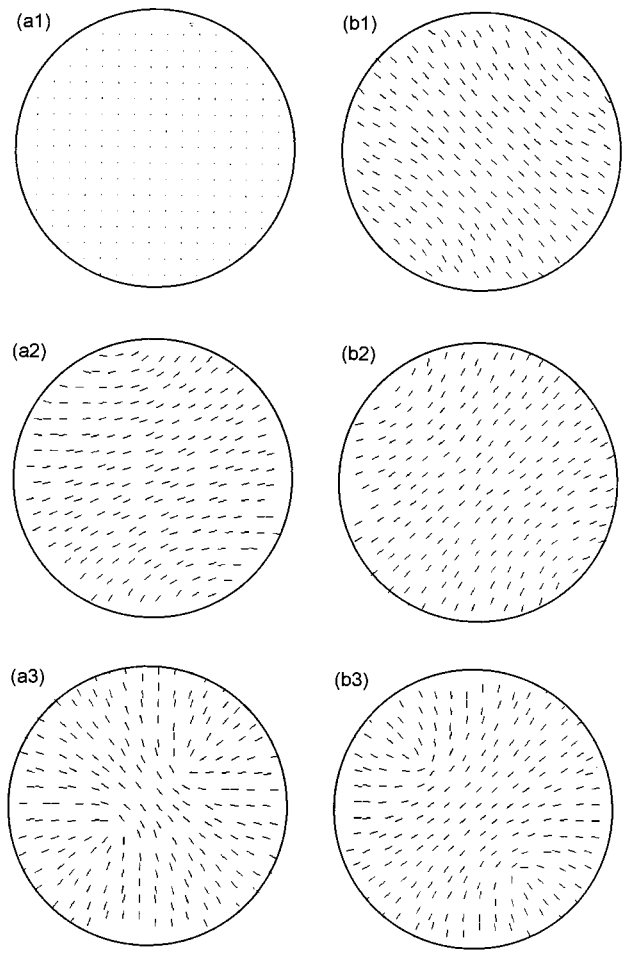

FIG. 3. Evolution of the nematic ordering (the director field representation) with increased ratio $\eta=J_s/J$ for $\varepsilon=0$ ($a1$: $\eta=0$, $a2$: $\eta=0.5$, $a3$: $\eta=2.0$) and $\varepsilon=0.3$ ($b1$: $\eta=0$, $b2$: $\eta=0.5$; $b3$: $\eta=2.0$); $N_r=8$.

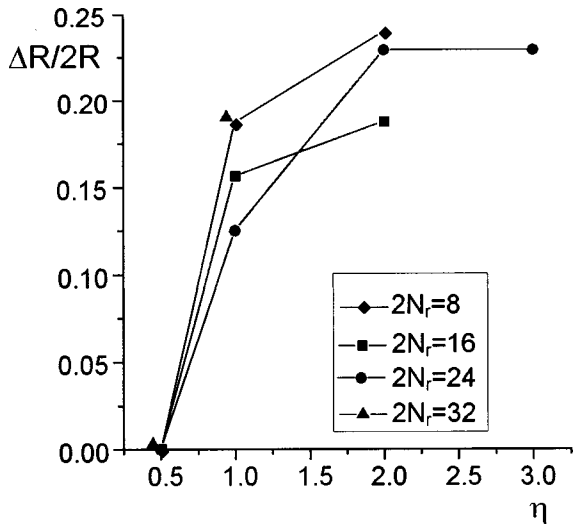

FIG. 4. Dependence $\Delta R=\Delta R(\eta)$ for different values of N_r.

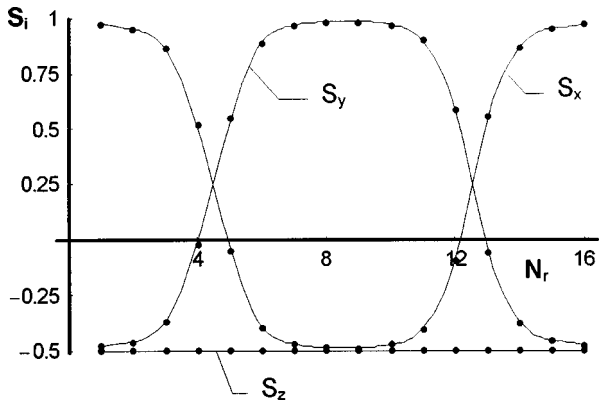

FIG. 5. The spatial dependence of eigenvalues S_i $(i=x,y,z)$ of the tensor order parameter along the line incorporating line defects in the azimuthal plane in the case of the PPLD structure. Biaxiality is substantial only near line defects. Exactly at defects the nematic order is uniaxial along the z axis. $\varepsilon=0$, $2N_r=16$, and $N_z=28$; the strong anchoring regime.

surface) elastic constants K_{13} and K_{24}, which can in general stabilize deformed nematic structures [35,39,41] even in case of zero anchoring strength. Skačej *et al.* [35] showed that, for large enough values of ε, the intrinsic anchoring favors planar anchoring in the planar geometry. We conjecture that in our case at $\varepsilon=0.3$ the anisotropy is strong enough so that the established planar intrinsic contribution to the anchoring dominates over the homeotropic external anchoring. This condition defines boundary conditions at $J_s\simeq 0$, and because of a curved surface enforces a deformed structure.

Note that a specific choice of lattice can introduce an artificial preference direction into the system. This can in turn strongly influence [35] details of the internal anchoring that become particularly important in the weak external anchoring regime. In our calculations we got rid of the preference axis using the procedure described above Eq. (4).

B. Defects

The points of strong distortions described above correspond to singular points [10] (i.e., dislocations or defects) in the continuum uniaxial picture. They are singular in the sense of a discontinuous change of the local director field orientation. At the singularity the director orientation is not uniquely defined, resulting in a vanishing value of the local macroscopic uniaxial orientational order parameter S. In a more complex biaxial continuum description (in terms of the tensor order parameter Q_{ij}) the evolution across the defect is gradual [24,42]. Therefore in this description the notion *defect* describes a strong local distortion, but nonsingular nematic order. (From the topological point of view a stable defect cannot be unfolded in a continuous way into a defectless structure.)

To illustrate the above discussion, in Fig. 5 we plot the spatial dependence of eigenvalues of the tensor order parameter in the PPLD structure. Local order parameters are obtained via diagonalization of the tensor $Q_{ij}=\langle(3n_in_j-\delta_{ij})/2\rangle$, where δ_{ij} is the Kronecker tensor, n_i is the ith component of the director field, and $\langle\cdots\rangle$ describes time averaging and averaging over first neighbors.

In Fig. 5, the variation of eigenvalues along the line in the azimuthal plane incorporating both line defects is shown. Let us assume that the x axis of the coordinate system points in this direction, and that the z axis is along the cylinder axis. The eigenvalues along the x, y, and z axes of the coordinate system are denoted by S_x, S_y, and S_z, respectively. The cases where two eigenvalues are equal correspond to uniaxial states. At the cylinder wall the nematic order is uniaxial along the radial direction (i.e., $S_y = S_z$). On approaching line defects the degeneracy between S_y and S_z is lifted, resulting in a biaxial nematic state. At defects sites the exchange of eigenvalues takes place. Consequently, there the nematic state is again uniaxial but with a negative uniaxial order parameter along the z axis [43]. On approaching the cylinder center, the uniaxial order along the y axis is progressively increased. Note that the eigenvalue S_z exhibits negligible spatial variations due to the extremely low temperature used in the model. In turn, in structures without defects the biaxiality is negligible.

C. Relaxation

The metastable ERPD structure was locked in in our simulations only if defects were separated for a distance d larger than $2R$. This result is in line with analytical predictions [32] obtained by Peroli and Virga. In their model the attraction force between adjacent defects is negligible (numerical simulations reveal exponentional decay with the distance) for $d > 2.2R$, and therefore the annihilation of defects is not expected within a reasonable simulation time.

An interesting demonstrative annihilation process is illustrated in Fig. 6. The LC ensemble was quenched from the isotropic phase. The parameters are chosen in such a way that the free energies of the ER ($F = F_{\mathrm{ER}}$) and PPLD ($F = F_{\mathrm{PPLD}}$) structures are similar, and $F_{\mathrm{ER}} < F_{\mathrm{PPLD}}$. Therefore, in the long run, the ER structure is stabilized. An intermediate stage, where the domain with the ER structure is surrounded with the domains exhibiting the PPLD structure, is shown in Fig. 6. The structure at the left consists of two line defects, each of topological charge $M = +\frac{1}{2}$. On approaching the ER domain the line defects gradually approach each other and finally merge into a single line defect of strength $M = +1$. This defect enables the LC to escape along the cylinder axis, providing continuous transformation into a domain with the ER structure. Note that the relative positions of line defects in both domains with PPLD structure are the same due to periodic boundary conditions. With time the ER domain grows at the expense of metastable surrounding domains. Details about this annihilation process will be published in a separate paper which will focus on the dynamics of the model.

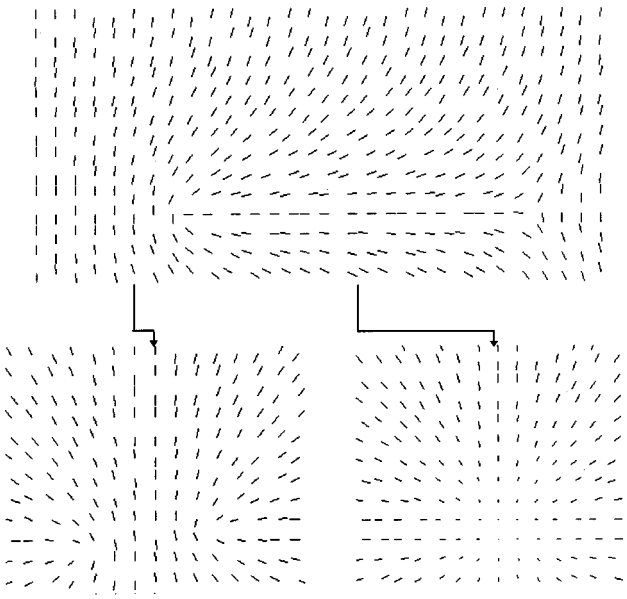

FIG. 6. An intermediate stage of relaxation process toward the ER structure. The LC was quenched from the isotropic phase. The figure presents an intermediate stage where the ER domain is enclosed by the domains with the PPLD structure. At later stages the ER domain fills the whole region. At the top a part of the (x,z) cross section incorporating the cylinder axis is shown. The position of the cylinder axis is evident from the central ER domain. Below this figure parts of the (x,y) cross sections of the PPLD (left) and ER (right) domain are shown. $2N_r = 32$, $N_z = 44$, strong anchoring regime. Number of sweeps is $N_s \approx 6000$. The ER structure was reached at approximately $N_s \approx 7000$.

D. Link between microscopic and macroscopic approaches

As mentioned in Sec. I, a lattice point in our model represents, in general, a group of molecules [18,20] in a real system. To estimate the actual size of the cylinders considered in our simulations, we relate predictions of our microscopic approach with the known results obtained in the continuum limit. Therefore we focus on Fig. 5, where the spatial evolution of the tensor order parameter eigenvalues are shown in the PPLD structure. In continuum language the depressed value of the order parameter at the defect site recovers to its bulk value on a scale given by the nematic correlation length ξ_n. In the case studied here (very low temperature), ξ_n is of the order of molecular dimensions a_o. Thus we conclude that in our case we are close to one-to one mapping. Thus a site in our calculation corresponds to one or 27 molecules [an ''interaction sphere'' in our model consists of 27 molecules; see the text above Eqs. (4)], as predicted by Chiccoli and co-workers [18–20,23].

Next we demonstrate that in the submicron regime the predictions for the structural details of both (microscopic and elastic) approaches reasonably agree. For this purpose we study structural details of the ER structure shown in Fig. 7 for $\varepsilon = 0$ for different anchoring strengths. In Fig. 7(a), the dependence of the spatial dependence of the ER director field (represented by Θ) is shown for different ratios η. The corresponding evolution of the surface orientation angle $\Theta_m = \Theta(r = R)$ for $N_r = 8$ is depicted in Fig. 7(b). Both $\Theta = \Theta(r)$ and $\Theta_m = \Theta_m(\eta)$ dependences are close to those predicted from the elastic approach. This indicates that not only qualitative but also quantitative predictions reached in the continuum picture work well even in the submicron regime studied.

From the obtained $\Theta_m = \Theta_m(\eta)$ dependence, some macroscopic quantities can be estimated at the AH-ER transition. Within the elastic theory, Θ_m evolves with anchoring strength as $\Theta_m = \arccos(d_e/R)$ for $R/d_e > 1$, and $\Theta_m = 0$ elsewhere. The surface extrapolation length [7] is defined as

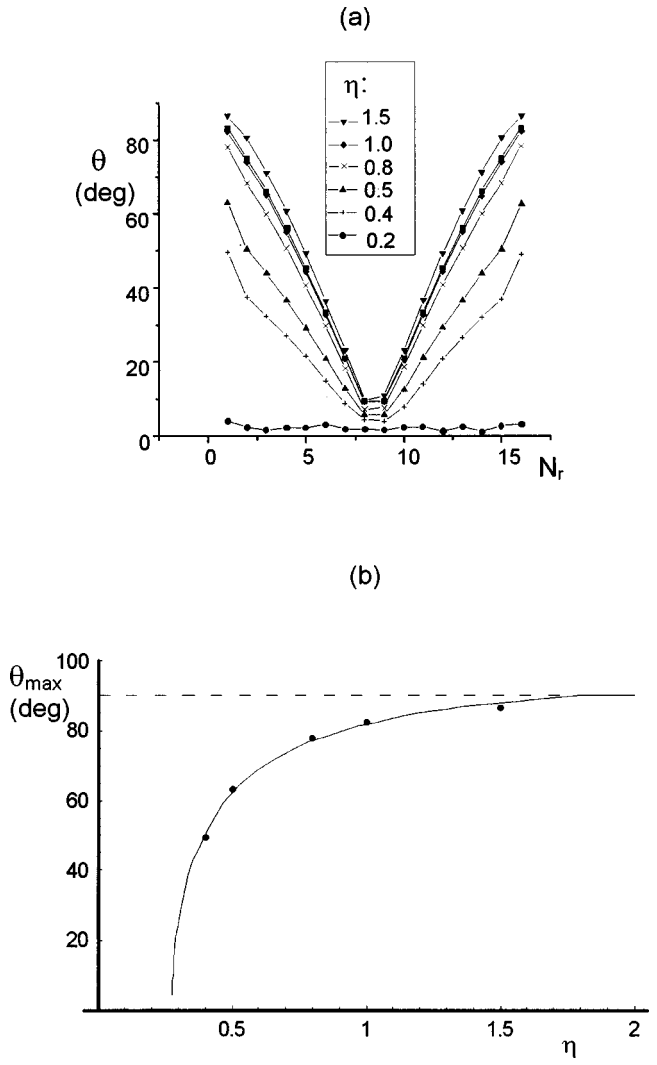

FIG. 7. (a) The spatial dependence $\Theta=\Theta(r)$ of the ER structure for different values of $\eta=J_s/J$. (b) Variation of the average surface angle Θ_m with η. Points: microscopic model calculations; full line: elastic theory prediction. The dimensionless parameter is defined as $\sigma=R/d_e=N_rC\eta$, where C is a proportional constant. The best match between the elastic and microscopic approaches is obtained for $N_rC\approx 5$.

$d_e=K/W_a$, where W_a describes the anchoring strength and K is the average nematic elastic constant. Assuming $R\propto N_r$, $W_a\propto J_s$, and $K\propto J$, one obtains $R/d_e=CN_rJ_s/J$, where C is a proportional constant. The best fit between the elastic and microscopic approach, shown in Fig. 7(b), is obtained for $N_rC\approx 5(1\pm 0.05)$. From the figure we infer that the transition between the AH and ER solution takes place at $J_s/J\approx 0.2(1\pm 0.05)$, that corresponds to $R/d_e=1$ in the elastic picture. Assuming $\xi_n\approx a_o$, we obtain the AH-ER transition at $d_e=R\approx 8a_o\approx 24$ nm, corresponding to $W_a\approx 10^{-4}$ J/m^2. In the estimation we set [7] $K\approx 5\times 10^{-12}$ J/m^2 and $a_o\approx 3$ nm, describing a typical nematic liquid crystal.

IV. CONCLUSIONS

We have analyzed the stability of nematic structures confined to a cylindrical capillary enforcing homeotropic anchoring using a molecular dynamics approach on a microscopic lattice model. The main purpose of the study was to test the applicability of continuum type approaches [7] (Landau–de Gennes and elastic approaches) in systems whose typical linear dimensions are well in the submicron region. In our calculations the cylindrical geometry was chosen because (i) it exhibits a reach palette of qualitatively different nematic structures, (ii) this simple geometry is admissible to rather nonsophisticated calculations and (iii) various experiments. The main results of our work are the following.

We have obtained different LC structures varying the cylinder size, anchoring strength, and anisotropy constant ε. Variation of ε affects ratios of the nematic elastic constants defined in the elastic theory. The range of their stability in most cases confirm predictions based on continuum approaches. The stable structures observed in the simulation were the planar radial (PR), the planar polar (PP), the planar polar with line defects (PPLD), the escaped radial (ER), the escaped radial with point defects (ERPD), and the axial homogeneous (AH) structure. For $\varepsilon=0$, corresponding in the elastic description to the approximation [40] of equal nematic elastic constants, either the AH (in the very weak anchoring regime), PP (weak anchoring regime) or PPLD and PR (strong anchoring regime) structure is obtained. The separation of line defects in the PPLD structure as a function of anchoring strength is calculated. For small enough R the line defects can merge resulting in the PR structure. In the elastic limit, (i.e., $R\gg\xi_n$) the ER structure is stable. In the case $\varepsilon>0$ the stability of the ER structure is pushed toward larger R, and the planar bipolar (PB) structure appears in the weak (external) anchoring regime.

For large enough value of the anisotropy constant ε ($\varepsilon\geqslant 0.3$) the PB structure is observed as a consequence of the internal [35] anchoring. It is caused by incomplete intermolecular interaction at the limiting surface. In general it enforces different easy axis than the external anchoring. We conjecture that for $\varepsilon\geqslant 0.3$ it enforces planar internal anchoring, dominating boundary conditions in the weak external anchoring regime. Because of the curved surface the resulting structure is deformed at $J_s\simeq 0$. Note that the intrinsic anchoring is inherent in our model, which is not the case in continuum type approaches.

In the regime of its potential realization the metastable ERPD structure is locked in only if adjacent defects as separated more than $2R$. This observation confirms analytical results by Peroli and Virga [32] predicting substantial force between point defects if their separation is less that $2.2R$.

The comparison of the results obtained in the microscopic and elastic approach roughly defines macroscopic parameters entering our model. For the ER structure we demonstrate a good match between approaches even in the regime where the applicability of the continuum approaches is questionable. We obtain a transition between ER and AH structures for $N_r=8$ at $J_s/J\approx 0.2$, corresponding to $R\approx 24$ nm and the anchoring strength $W_a\approx 10^{-4}$ J/m^2. A lattice point in simulation corresponds to one or 27 molecules.

In conclusion, we would like to emphasize that despite using rather primitive model restricted to a lattice, we obtain reasonable results justifying continuum predictions. This

indicates that the simple model used contains essential ingredients responsible for the observed macroscopic behavior. However, in order to gain better quantitative agreement a more sophisticated microscopic model is needed (e.g., allowing translational degrees of freedom of the interacting ''molecules'').

ACKNOWLEDGMENTS

We thank E. Virga and T. J. Sluckin for useful discussions and we gratefully acknowledge the financial support of the Slovenian Ministry of Science and Technology (Grants No. J1-7069, J2-7609-0589-96) and the European Community Project (ERB-FMRX-CT98-0209).

[1] P. E. Cladis and M. Kleman, J. Phys. (France) **33**, 591 (1972).
[2] E. Williams, P. E. Cladis, and M. Kleman, Mol. Cryst. Liq. Cryst. **21**, 355 (1973).
[3] B. J. Liang and S. H. Chen, Jpn. J. Appl. Phys. **30**, L1955 (1991).
[4] G. S. Iannacchione, G. P. Crawford, J. W. Doane, and D. Finotello, Mol. Cryst. Liq. Cryst. **222**, 205 (1992).
[5] C. Cramer, T. Cramer, F. Kremer, and R. Stannarius, J. Chem. Phys. **106**, 3730 (1997).
[6] G. P. Crawford, D. W. Allender, and J. W. Doane, Phys. Rev. A **45**, 8693 (1992), and references therein.
[7] P. G. de Gennes and J. Prost, *The Physics of Liquid Crystals* (Oxford University Press, Oxford, 1993).
[8] S. Kralj and S. Žumer, Phys. Rev. E **51**, 366 (1995).
[9] M. Ambrožič and S. Žumer, Phys. Rev. E **54**, 5187 (1996).
[10] M. Kleman, *Points, Lines and Walls* (Wiley, Chichester, 1983).
[11] *Liquid Crystals in Complex Geometries Formed by Polymer and Porous Networks*, edited by G. P. Crawford and S. Žumer (Taylor and Francis, London, 1996).
[12] G. S. Iannacchione, J. T. Mang, S. Kumar, and D. Finotello, Phys. Rev. Lett. **73**, 2708 (1994).
[13] R. O. Crawford, G. P. Crawford, J. W. Doane, S. Žumer, M. Vilfan, and I. Vilfan, Phys. Rev. E **48**, 1998 (1993).
[14] N. A. Clark, T. Bellini, R. M. Malzbender, B. N. Thomas, A. G. Rappaport, C. D. Muzny, D. W. Schaefer, and L. Hrubesh, Phys. Rev. Lett. **71**, 3505 (1993).
[15] F. M. Aliev, Kristallografiya **33**, 969 (1988) [Sov. Phys. Crystallogr. **33**, 573 (1988)].
[16] G. S. Iannacchione, G. P. Crawford, S. Žumer, J. W. Doane, and D. Finotello, Phys. Rev. Lett. **71**, 2595 (1993).
[17] S. Kralj, A. Zidanšek, G. Lahajnar, S. Žumer, and R. Blinc, Phys. Rev. E **57**, 3021 (1998).
[18] E. Berggren, C. Zannoni, C. Chiccoli, P. Pasini, and F. Semeria, Phys. Rev. E **50**, 2929 (1994).
[19] C. Chiccoli, P. Pasini, F. Semeria, Phys. Lett. A **150**, 311 (1990).
[20] C. Chiccoli, P. Pasini, F. Semeria, E. Berggren, and C. Zannoni, Mol. Cryst. Liq. Cryst. **290**, 237 (1996).
[21] V. Palermo, F. Biscarini, and C. Zannoni, Phys. Rev. E **57**, R2519 (1998).
[22] C. Chiccoli, O. D. Lavrentovich, P. Pasini, and C. Zannoni, Phys. Rev. Lett. **79**, 4401 (1997).
[23] T. Bellini, C. Chiccoli, P. Passini, and C. Zannoni, Mol. Cryst. Liq. Cryst. **290**, 227 (1996).
[24] A. Sonnet, A. Kilian, and S. Hess, Phys. Rev. E **52**, 718 (1995).
[25] P. Ziherl and S. Žumer, Phys. Rev. E **54**, 1592 (1996).
[26] G. Barbero, Mol. Cryst. Liq. Cryst. **195**, 199 (1991).
[27] F. J. Vesely, *Computational Physics* (Plenum, New York, 1994).
[28] B. Jerome, Rep. Prog. Phys. **54**, 351 (1991), and references therein.
[29] N. D. Mermin, Rev. Mod. Phys. **51**, 591 (1976).
[30] G. E. Volovik and O. D. Lavrentovich, Zh. Éksp. Teor. Fiz. **85**, 1997 (1983) [Sov. Phys. JETP **58**, 1159 (1983)].
[31] J. Bezić and S. Žumer, Liq. Cryst. **14**, 1695 (1993).
[32] G. G. Peroli and E. G. Virga, Phys. Rev. E **54**, 5235 (1996); **56**, 1819 (1997).
[33] R. D. Williams, J. Phys. A **19**, 3211 (1986).
[34] P. A. Lebwohl and G. Lasher, Phys. Rev. A **6**, 426 (1972).
[35] G. Skačej, V. M. Pergamenshchik, A. L. Alexe-Ionescu, G. Barbero, and S. Žumer, Phys. Rev. E **56**, 571 (1997), and references therein.
[36] D. L. Ermak, J. Chem. Phys. **62**, 4189 (1975).
[37] R. Ying and M. H. Peters, J. Chem. Phys. **95**, 1234 (1991).
[38] S. Kralj and S. Žumer, Phys. Rev. E **54**, 1610 (1996).
[39] S. Kralj and S. Žumer, Phys. Rev. A **45**, 2461 (1992).
[40] A. L. Alexe Ionescu, R. Barberi, G. Barbero, and M. Giocondo, Phys. Lett. A **190**, 109 (1994).
[41] V. M. Pergamenshchik, Phys. Rev. E **48**, 1254 (1993).
[42] N. Shopol and T. J. Sluckin, Phys. Rev. Lett. **59**, 2582 (1987).
[43] E. Penzenstadler and H. R. Trebin, J. Phys. (France) **50**, 1025 (1989).